Polyhedron 54 (2013) 1–7

Contents lists available at SciVerse ScienceDirect

Polyhedron

journal homepage: www.elsevier.com/locate/poly

Synthesis, crystal structure and photoluminescence of a binuclear complex of europium(III) containing 3,5-dicarboxypyrazolate and succinate

Marcelo G. Lahoud [a], Lippy F. Marques [b], Patrícia B. da Silva [a], Caio A.S. de Jesus [a], Cecilia C.P. da Silva [c], Javier Ellena [c], Rafael S. Freitas [d], Marian R. Davolos [a], Regina C.G. Frem [a,*]

[a] Instituto de Química, Unesp – Univ Estadual Paulista, 14801-970 Araraquara, SP, Brazil
[b] Departamento de Química-ICE, Universidade Federal de Juiz de Fora, Juiz de Fora-MG 36036-330, Brazil
[c] Instituto de Física, Universidade de São Paulo, São Carlos 13560-970, SP, Brazil
[d] Instituto de Física, Universidade de São Paulo, São Paulo 05315-970, SP, Brazil

ARTICLE INFO

Article history:
Received 2 October 2012
Accepted 29 January 2013
Available online 4 February 2013

Keywords:
3,5-Dicarboxypyrazolate
Succinate
Europium(III) ion

ABSTRACT

The new europium binuclear complex $[Eu_2(dcpz)_2(suc)(H_2O)_8]\cdot(H_2O)_{1.5}$ (dcpz = 3,5-dicarboxypyrazolate and suc = succinate) has been synthesized and structurally characterized by single crystal X-ray diffraction methods. The binuclear complex crystallizes in the triclinic space group $P\bar{1}$ and consists of two lanthanide ions linked by two different bridging organic ligands. 3D supramolecular framework is constructed by hydrogen bonds. The compound shows strong red emission under UV excitation at room temperature associated to IL transitions indicating a ligand to metal energy transfer mechanism since the triplet energy level lies higher than that of europium $^5D_0$ level. Magnetic susceptibility studies showed weak temperature dependence characteristic of the Van Vleck paramagnetism.

1. Introduction

The unique electronic structures of lanthanide cations linked by organic ligands find in recent years an increasing number of important technological applications [1] ranging from nuclear magnetic resonance imaging [2] to luminescent materials [3]. According to the emission features of the Ln^{3+} ion, luminescent sensors, optical fiber lasers and amplifiers [4] as well multicolor displays and organic light-emitting diodes (OLEDs) [5] have been prepared.

The lanthanide-based compounds have wide luminescent material use due to their extremely narrow emission bands combined with relatively long excited-state lifetimes that result from intraconfigurational 4f–4f transitions [6]. However the impositions generated by the selection rules bring about low molar absorptivity and emission intensity for these systems. This fact can be overcome with the coordination of organic ligands that transfer energy to the lanthanide ions (antenna effect) thus generating very efficient luminescent materials [7,8].

From this point of view, dicarboxylate ligands are a good choice since they may contain chromophore groups. Besides that, these O-donor ligands efficiently coordinate Ln^{3+} ions leading to discrete molecules or coordination polymers [9]. These compounds in turn can be held together by H-bonds that act as supramolecular glue in the construction of more complex supramolecular assemblies [10].

Both succinate anions and pyrazoledicarboxylate ligands used in this work are convenient building blocks for construction of metallosupramolecules. However, based on rare earth systems built from these two different carboxylate bridging ligands have received less attention in the literature [11].

Concerning the formation of europium (III) compounds it is worth mentioning the reports of Wu et al. [12] and Zhang et al. [13] that describe the hydrothermal synthesis of the luminescent MOF $[Eu(dcpz)(ox)_{0.5}(H_2O)_2]\cdot H_2O$ containing oxalate anion (ox) and 3,5-dicarboxypyrazole (dcpz) ligand.

In relation to similar Eu^{3+} systems containing only one of the ligands, Xia et al. [14] reported the synthesis under hydrothermal conditions of the compound $[Eu_2(dcpz)_3(H_2O)_3]\cdot 3H_2O$ that shows a 2D double-decker framework. On the other hand the complex $[Eu_2(suc)_3(H_2O)_2\cdot 0.5H_2O$ has been synthesized and structurally characterized through X-ray diffraction analysis [15]. This compound is constructed by succinate bridging chains of edge-sharing $EuO_8(H_2O)$ polyhedra to form a 3D network structure [16].

In this paper, we reported for the first time the synthesis of $[Eu_2(dcpz)_2(suc)(H_2O)_8]\cdot(H_2O)_{1.5}$ obtained from the reaction of Eu(III) ions with 3,5-dicarboxypyrazolate and succinate (suc) ligands (see Fig. 1). In this case binuclear discrete units are formed and connected by complementary dcpz-H_2O and H_2O–H_2O hydrogen-bonds forming a 3D supramolecular assembly. Antenna effect is observed in this compound since that the ligands transfer energy to the europium level leading to a strong red emission. Magnetic

* Corresponding author. Tel.: +55 16 33019623.
E-mail address: rcgfrem@iq.unesp.br (R.C.G. Frem).

0277-5387/$ - see front matter © 2013 Elsevier Ltd. All rights reserved.
http://dx.doi.org/10.1016/j.poly.2013.01.031

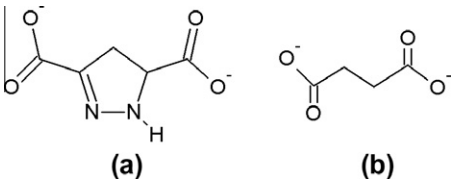

Fig. 1. Structural formulae of the ligands (a) 3,5-dicarboxypyrazolate and (b) succinate.

studies were also realized and revealed the nearly temperature independent behavior of the susceptibility below 100 K.

2. Experimental

2.1. Materials and measurements

All synthetic work was performed in air and at room temperature. $EuCl_3{\cdot}6H_2O$, 3,5-pyrazoledicarboxylic acid and sodium succinate were obtained from Aldrich® and used as received. Elemental analyses for C, H and N were carried out using a CE Instruments EA1110 CHNS-O microanalyzer. IR spectra were recorded with a NICOLET model SX-FT Impact 400 spectrophotometer using KBr pellets in the wavenumber range of 4000–400 cm^{-1} with an average of 128 scans and 4 cm^{-1} of spectral resolution. Thermogravimetric analysis (6.006 mg of the compound) was performed on TG 60. Sample was heated at 10 °C/min from room temperature to 800 °C in a dynamic air atmosphere (flow rate = 100 mL/min). Diffuse reflection (DR) spectra were acquired on a Cary 500 spectrophotometer in the range from 230 to 800 nm with spectral resolution of 1 nm. The luminescence excitation and emission spectra were obtained with a Horiba Jobin Yvon Model Fluorolog FL3-222 spectrophotometer equipped with a R928 Hamamatsu photomultiplier and 450 W Xe lamp as the excitation source using a front face mode. The spectra were corrected with respect to the Xe lamp intensity and spectrometer response. Measurements of emission decay were performed with the same equipment by using a pulsed Xe (3 μs bandwidth) source. The dc magnetic susceptibility was measured with a superconducting quantum interference device magnetometer (Quantum Design MPMS) on cooling over T = 314–2 K in an applied magnetic field of H = 1 T.

2.2. Synthesis of $[Eu_2(dcpz)_2(suc)(H_2O)_8]{\cdot}(H_2O)_{1.5}$

Sodium succinate (0.273 mmol, 44 mg) was added to europium chloride (0.136 mmol, 50 mg) in water (20 mL) generating a colorless solution. Then a solution containing NaOH (0.136 mmol) and H_2dcpz (0.136 mmol, 24 mg) was added to the initial reaction mixture. The resulting solution was allowed to stand at room temperature open to the air. After three days, translucent crystals suitable for single crystal X-ray diffraction were obtained. Yield: 49%. *Anal.* Calc. for $C_{14}H_{27}Eu_2N_4O_{21.5}$: C, 18.70; H, 3.03; N, 6.23. Found: C, 18.84; H, 2.81; N, 6.04%.

2.3. X-ray diffraction data

The X-ray experiments were performed at room temperature on an Enraf–Nonius Kappa-CCD diffractometer (95 mm CCD camera on φ-goniostat) using graphite-monochromated MoKα radiation (0.71073 Å). Final unit cell parameters were based on all reflections. Data collection was carried out using the COLLECT program [17]. Integration and scaling of the reflections were performed with the HKL Denzo–Scalepack system of programs [18]. Gaussian absorption correction was applied [19]. The structure was solved by direct methods using SHELXS-97 [20]. The model was refined by full-matrix least-squares on F^2 with SHELXL-97 [20]. All hydrogen atoms were stereochemically positioned and refined with the riding model [20]. Hydrogen atoms of the water molecules were set isotropic with a thermal parameter 50% greater than the equivalent isotropic displacement parameter of the O-atom to which they are bonded. ORTEP diagram was prepared with ORTEP-3 for Windows [21] and VESTA [22] software was used to prepare artwork representations for publication. PLATON [23] software was used to validate the crystallographic data. The main crystal, collection and structure refinement data for $[Eu_2(dcpz)_2(suc)(H_2O)_8]{\cdot}(H_2O)_{1.5}$ are summarized in Table 1.

Table 1
Crystallographic data and structure refinement parameters for $[Eu_2(dcpz)_2(suc)(H_2O)_8]{\cdot}(H_2O)_{1.5}$.

Empirical formula	$C_{14}H_{27}N_4O_{21.5}Eu_2$
Formula weight	899.32
T (K)	293(2)
Wavelength (Å)	0.71073
Crystal system	Triclinic
Space group	$P\bar{1}$
Unit cell dimensions	
a (Å)	10.1629(1)
b (Å)	11.4510(1)
c (Å)	13.5682(2)
α (°)	73.5098(7)
β (°)	69.8237(6)
γ (°)	64.0072(6)
V (Å^3)	1315.6(2)
Z	2
D_{calc} (Mg/m^3)	2.270
Absorption coefficient (mm^{-1})	4.827
F(000)	874
Crystal size (mm^3)	0.22 × 0.15 × 0.07
θ Range (°)	3.14–25.69
Index ranges	−12,12; −13,13; −16,16
Reflections collected	23861
Reflections collected/unique (R_{int})	9379/4963 (0.0152)
Completeness to theta = 25.71°	99.3%
Absorption correction method	gaussian
Max. and min. transmission factors	0.7287 and 0.4165
Refinement method	full-matrix least-squares on F^2
Data/restraints/parameters	4963/0/379
Goodness-of-fit on (GOF) F^2	1.124
Final R indices [$I > 2\sigma(I)$]	R_1 = 0.0192, wR_2 = 0.0449
R indices (all data)	R_1 = 0.0203, wR_2 = 0.0455
Largest difference in peak and hole (e Å^{-3})	0.863 and −0.703

3. Results and discussion

3.1. Synthesis considerations

As mentioned earlier generally this class of compounds has been prepared under solvothermal conditions. However, in this work single crystals were obtained by liquid diffusion under aqueous media and normal pressure conditions. Besides its friendly nature, the solvent molecules could also act as ligands and H-bond donor/acceptor groups in the solid. The deprotonation of pyrazolic ligands could be achieved by the addition of sodium hydroxide and the molar ratio between this ligand and the metal (1:1) was in the correct stoichiometric ratio for the reaction. However excess of succinate anion remained in solution and the open coordination sites of Eu(III) ion was filled with eight water molecules.

3.2. Crystal structure of $[Eu_2(dcpz)_2(suc)(H_2O)_8](H_2O)_{1.5}$

Fig. 2 depicts an ORTEP type view of the asymmetric unit of the $[Eu_2(dcpz)_2(suc)(H_2O)_8]{\cdot}(H_2O)_{1.5}$ complex, showing selected atoms labeling and the 50% probability ellipsoids. Table 2 shows a selected list of bond length and angles. The compound crystallizes

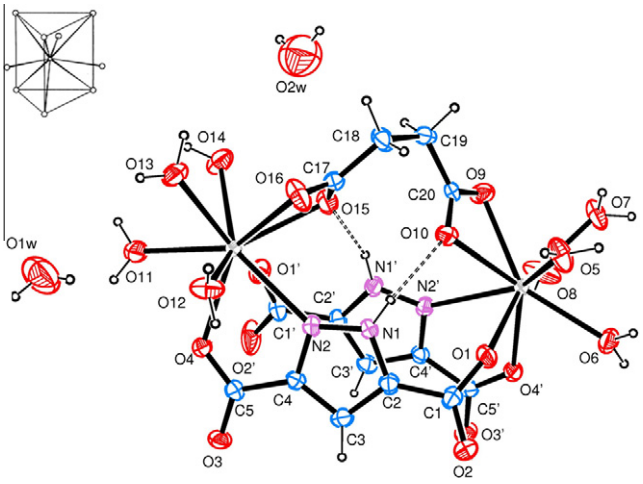

Fig. 2. ORTEP-3 [21] type view of the asymmetric unit of $[Eu_2(dcpz)_2(suc)(H_2O)_8]\cdot(H_2O)_{1.5}$, showing the atoms labeling and the 50% probability ellipsoids, and the two intramolecular hydrogen bonds. (Inset: coordination geometry of europium(III)).

in the triclinic space group $P\bar{1}$. (The asymmetric unit consists of a binuclear compound, composed by two europium(III) ions, a succinate anion, two pyrazolic ligands, eight coordinated water molecules and 1.5 crystallization water. The molecular conformation results in the formation of a cage whose sides are formed by the three ligands molecules. The coordination number of Eu^{3+} is nine and the coordination polyhedron can be best described as a tricapped trigonal prism (see inset of Fig. 2) like in the succinate-complexes $[Eu_2(suc)_3(H_2O)_2]\cdot xH_2O$ [15,16].

The succinate anion exhibits chelating-bidentate coordination fashion in which each carboxylate group chelates one europium center. The Eu–O bond lengths, ranging from 2.455 to 2.508 Å, are similar to those reported for $[Eu_2(suc)_3(H_2O)_2].H_2O_n$ (2.463–2.537 Å), which shows the same succinate coordination mode [16]. As also illustrated in Fig. 2, the two 3,5-dicarboxypyrazolate ligands exhibit, following the classification presented by Klingele et al. [24], the 1:1 polymeric coordination mode in which each dcpz molecule acts as a N2,O4-chelating ligand for one lanthanide ion while bonded only via the O1 atom to the other one. The average Eu–O1 bond length, 2.371 Å, is in agreement with the mean value found for $[Eu_2(dcpz)_3(H_2O)_6]$, 2.379 Å [25]. It is worth mentioning that two Eu(III) complexes containing this same ligand and oxalate anion with formula $[Eu(dcpz)(ox)_{0.5}(H_2O)_2]\cdot H_2O$ already reported in the literature [12,13] form three-dimensional metal–organic frameworks in which the dcpz ligands exhibit a very different bridging coordination modes from that described in this work. For this reason, and for the fact that the oxalate is smaller than the succinate anion, the Eu–Eu distance is 4.40 Å for $[Eu(dcpz)(ox)_{0.5}(H_2O)_2]\cdot H_2O$ [13] while in the binuclear compound described in this work it is 6.9515(6) Å. Intramolecular π···π face-to-face stacking interactions are present between the pyrazolic rings in the binuclear complex with a centroid to centroid distance of 3.394(2) Å, within the range of expected values for this kind of interaction in metal complexes with aromatic nitrogen-containing ligands in 3.3–3.8 Å [26]. Two N–H···O intramolecular hydrogen bonds, N1′–H1′···O15 and N1–H1···O10, between the oxygen atoms of the succinate groups (O15 e O10) and hydrogen atoms from pyrazolic ligands (N1′ e N1) are also observed in the binuclear complex (see Fig. 2).

The units of the binuclear complex $[Eu_2(dcpz)_2(suc)(H_2O)_8]\cdot(H_2O)_{1.5}$ make several O–H···O strong intermolecular hydrogen bonds through the oxygen atoms of the dcpz-carboxylates ligand

Table 2
Selected bond lengths (Å) and angles (°) for $[Eu_2(dcpz)_2(suc)(H_2O)_8]\cdot(H_2O)_{1.5}$.

Eu1–O1	2.369(2)
Eu1–O8	2.388(2)
Eu1–O5	2.443(2)
Eu1–O6	2.447(2)
Eu1–O4′	2.451(2)
Eu1–O9	2.455(2)
Eu1–O10	2.504(2)
Eu1–O7	2.515(2)
Eu1–N2′	2.607(2)
Eu2–O1′	2.372(2)
Eu2–O12	2.385(2)
Eu2–O14	2.432(2)
Eu2–O4	2.448(2)
Eu2–O11	2.452(2)
Eu2–O16	2.475(2)
Eu2–O15	2.508(2)
Eu2–O13	2.551(2)
Eu2–N2	2.599(2)
O1–Eu1–O8	143.55(8)
O1–Eu1–O5	75.66(8)
O8–Eu1–O5	136.34(8)
O1–Eu1–O6	81.76(8)
O8–Eu1–O6	90.03(10)
O5–Eu1–O6	75.32(8)
O1–Eu1–O4′	75.25(8)
O8–Eu1–O4′	68.47(8)
O5–Eu1–O4′	138.39(8)
O6–Eu1–O4′	71.63(7)
O1–Eu1–O9	126.37(7)
O8–Eu1–O9	78.30(9)
O5–Eu1–O9	90.21(8)
O6–Eu1–O9	144.55(8)
O4′–Eu1–O9	131.16(8)
O1–Eu1–O10	74.88(7)
O8–Eu1–O10	127.16(9)
O5–Eu1–O10	68.33(8)
O6–Eu1–O10	140.49(8)
O4′–Eu1–O10	129.72(7)
O9–Eu1–O10	52.10(7)
O1–Eu1–O7	141.60(8)
O8–Eu1–O7	68.10(8)
O5–Eu1–O7	68.52(8)
O6–Eu1–O7	76.33(8)
O4′–Eu1–O7	125.01(8)
O9–Eu1–O7	68.24(8)
O10-Eu1–O7	103.27(7)
O1–Eu1–N2′	80.41(8)
O8–Eu1–N2′	80.66(9)
O5–Eu1–N2′	137.66(8)
O6–Eu1–N2′	134.86(8)
O4′–Eu1–N2′	63.83(7)
O9–Eu1–N2′	76.57(8)
O10–Eu1–N2′	72.00(7)
O7–Eu1–N2′	136.50(8)
O1′–Eu2–O12	144.14(8)
O1′–Eu2–O14	75.76(8)
O12–Eu2–O14	138.49(8)
O1′–Eu2–O4	76.08(8)
O12–Eu2–O4	70.25(8)
O14–Eu2–O4	135.31(8)
O1′–Eu2–O11	85.29(9)
O12–Eu2–O11	94.21(9)
O14–Eu2–O11	74.04(8)
O4–Eu2–O11	69.71(7)
O1′–Eu2–O16	123.27(7)
O12–Eu2–O16	75.95(8)
O14–Eu2–O16	89.90(9)
O4–Eu2–O16	134.71(8)
O11–Eu2–O16	143.15(8)
O1′–Eu2–O15	72.02(7)
O12–Eu2–O15	122.88(8)
O14–Eu2–O15	69.72(8)
O4–Eu2–O15	130.88(7)
O11–Eu2–O15	140.84(8)
O16–Eu2–O15	51.73(7)

(*continued on next page*)

O1′–Eu2–O13	144.28(8)
O12–Eu2–O13	67.98(8)
O14–Eu2–O13	70.52(8)
O4–Eu2–O13	121.58(7)
O11–Eu2–O13	74.59(9)
O1′–Eu2–N2	78.40(8)
O12–Eu2–N2	76.17(8)
O14–Eu2–N2	139.91(8)
O4–Eu2–N2	64.18(7)
O11–Eu2–N2	133.49(8)
O16–Eu2–N2	79.29(8)
O15–Eu2–N2	73.44(7)
O13–Eu2–N2	136.38(9)
O16–Eu2–O13	68.77(8)
O15–Eu2–O13	105.93(7)

Table 3
H-bonds parameters (Å, °) in $[Eu_2(dcpz)_2(suc)(H_2O)_8]\cdot(H_2O)_{1.5}$ crystal structure.

D–H···A	d(D–H)	d(H···A)	d(D···A)	<(DHA)
Intramolecular				
N(1′)–H(1′)···O(15)	0.86	2.13	2.921(3)	152.7
N(1)–H(1)···O(10)	0.86	2.08	2.869(5)	151.7
Intermolecular				
O(5)–H(5B)···O(4)^{i}	0.89	1.93	2.800(3)	169.0
O(6)–H(6A)···O(3)^{i}	0.85	1.85	2.692(4)	172.0
O(7)–H(7A)···O(2′)^{i}	0.88	1.80	2.687(4)	179.0
O(8)–H(8A)···O(9)^{ii}	0.90	1.77	2.665(4)	175.0
O(8)–H(8B)···O(3′)^{iii}	0.89	1.87	2.737(4)	166.0
O(11)–H(11B)···O(3′)^{iv}	0.85	1.95	2.761(4)	160.0
O(12)–H(12A)···O(16)^{v}	0.85	1.83	2.690(4)	173.4
O(12)–H(12B)···O(3)^{vi}	0.85	1.87	2.716(4)	177.0
O(13)–H(13A)···O(2)^{vii}	0.79	2.05	2.822(3)	162.0
O(13)–H(13B)···O(6)^{vii}	0.94	1.98	2.916(4)	174.0
O(14)–H(14B)···O(4′)^{vii}	0.85	1.89	2.719(3)	165.0

Symmetry transformations used to generate equivalent atoms: i: x, $1+y$, z; ii: $-x$, $2-y$, $1-z$; iii: $-1-x$, $2-y$, $1-z$; iv: $1+x$, $-1+y$, z; v: $-x+1$, $-y+1$, $-z$, vi: $-x$, $1-y$, $-z$; vii:$1+x$, $-1+y$, z.

(the one that is free as well as the one the is coordinated) and a coordinated water molecules (see Table 3). These interactions form a bi-dimensional layer on the ab plane as shown in the Fig. 3a. It is interesting to emphasize that these intermolecular interactions form several interesting supramolecular synthons [27]. One of this synthons is built by two water molecules coordinated to the same metal ion linked to two oxygen atoms of the same dcpz ligand (one free and one coordinated to the metal). Two of these synthons are present in the supramolecular structure that form the ab layers, one is the pair formed by O11–H11B···O3′^{iv} and O14–H14B···O4′^{vi}, and the other one is the pair formed by O5–H5B···O4 and O6–H6B···O3, respectively. The water molecule O11 acts, at the same time, as a hydrogen bond acceptor of an interaction with the coordinated water molecule O7, which is also a donor of another hydrogen bond with a free oxygen atom of a dcpz ligand bonded to the same metal ion, O2′. Finally, the water molecule O13 acts as a hydrogen bond donor of two intermolecular interactions. One of these interactions links to the water molecule O6 and the other one with the free oxygen atom of the dcpz ligand bonded to the same metal ion, O2.

The layers formed in the ab plane are stacked along the c axis, constituting a three-dimensional supramolecular structure as shown in Fig. 3b. In Fig. 4, it is possible to observe that due the symmetry of the crystalline system, two different types of layers are intercalated along the c axis: one layer with the gap of the cage turned to the [0 1 0] direction (purple in Fig. 4) and one layer with the gap of the cage turned to the [0 −1 0] direction (yellow in Fig. 4). The adjacent layers are held together basically by three O–H···O hydrogen bonds (see Fig. 4). The O8–H8A···O9′ interaction link one coordinated water molecule O8 and the oxygen atom

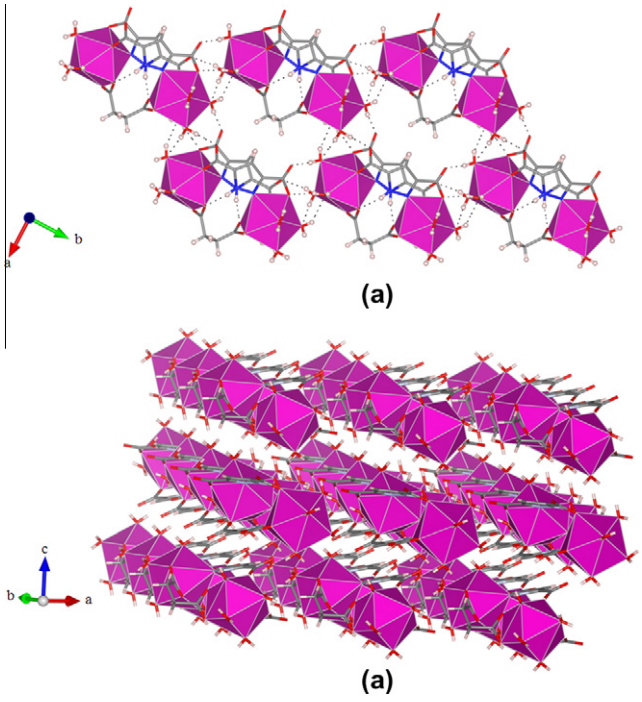

Fig. 3. Crystal packing of $[Eu_2(dcpz)_2(suc)(H_2O)_8]\cdot(H_2O)_{1.5}$ (a) view along the c axis, showing the formation of a bi-dimensional structure, and (b) along the ab plane, showing the construction of a three-dimensional network. Crystallization water molecules were omitted for clarity.

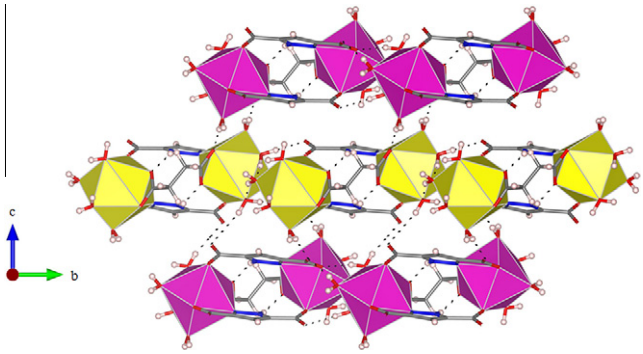

Fig. 4. Intercalated layers of $[Eu_2(dcpz)_2(suc)(H_2O)_8]\cdot(H_2O)_{1.5}$, evidencing in purple molecules with the gap of the cage turned to the [0 1 0] direction and in yellow molecules with the gap of the cage turned to the [0 −1 0] direction. Crystallization water molecules were omitted for clarity (Colour online).

O9 of the succinate ligand, forming a centrosymmetric dimer. This interaction links one purple layer to the next yellow one. At the same time, a similar pair of centrosymmetric interactions form dimers that links this yellow layer to the next purple one trough the O12–H12A···O16 hydrogen bond. The layers are also held together by the O12–H12B···O3 and O5–H5B···O2 hydrogen bonds, involving water molecules coordinated to the metal together with the oxygen of the free dcpz-carboxylate.

3.3. Infrared spectroscopy (IR)

The most relevant aspect for the IR spectrum (Figure S1 in Supplementary Material) of the europium compound is concerned with the values of the asymmetric and symmetric stretching frequencies for the COO^- groups. In this class of compounds, the difference between $\nu_{asym}(COO^-)$ and $\nu_{sym}(COO^-)$ ($\Delta\nu$) in comparison

to the corresponding values in ionic species is currently employed to determine a characteristic coordination mode of carboxylate group [28]. Eu^{3+} binuclear complex spectrum shows absorption bands at 1625 and 1359 cm^{-1} assigned to ν_{asym} and ν_{sym} stretching modes, respectively, giving $\Delta\nu = 266\ cm^{-1}$. This value is greater than the value of ionic specie Na_2dcpz ($\Delta\nu = 226\ cm^{-1}$) suggesting that the carboxylate group of dcpz ligand acts in a monodentate coordination mode. Similarly for the suc ligand, absorption bands around 1537 and 1435 cm^{-1} may be attributed to the ν_{asym} and ν_{sym} stretching modes, respectively. The calculated value of $\Delta\nu = 102\ cm^{-1}$ is closed to the value expected for a chelating coordination mode of the carboxylate group in the suc ligand [29].

A broad band is observed in the 3617–2994 cm^{-1} region which is characteristic of the ν(NH) and ν(CH) stretching vibrations attributed to the dcpz ligand and ν(OH) stretching vibration, indicating the presence of water molecules in accordance to the thermal analysis results. The absorption band at 516 cm^{-1} may be attributed to γNH of dcpz ligand and is not displaced when compared to the free ligand, suggesting that the nitrogen atoms of the pyrazole ring is not coordinated to the metal center as confirmed by X-ray diffraction.

3.4. Diffuse reflectance (DR) spectra and photoluminescence (PL) studies

DR spectra of Eu^{3+} complex and its precursors shown in Fig. 5 present characteristic bands of ligands and Eu^{3+} ion. The different ligands present wide and intense bands in the UV region, the carbonyl intra-ligand (IL) succinate begins at ~240 nm and the pyrazole ring and carbonyl at 280 nm. The Eu^{3+} complex also present a wide and intense absorption band shifted to longer wavelength, ~340 nm, due to the double bond weakening. However wide bands in this UV region are currently assigned to ligand to metal charge transfer transitions (LMCT) and probably in this case it can be also attributed to a N–Eu, at high energy and O–Eu at ~275 nm [30]. Characteristic absorption bands due to the transition from the ground-state to the excited states of the Eu^{3+} ion are observed, where peaks at 318, 362, 375, 380, 395, 415, 465, 525, 535, 579 and 591 nm are assigned to $^7F_0 \rightarrow {}^5H_6$, $^7F_0 \rightarrow {}^5D_4$, $^7F_0 \rightarrow {}^5G_6$, $^7F_0 \rightarrow {}^5G_5$, $^7F_0 \rightarrow {}^5L_6$, $^7F_0 \rightarrow {}^5D_3$, $^7F_0 \rightarrow {}^5D_2$, $^7F_0 \rightarrow {}^5D_1$, $^7F_1 \rightarrow {}^5D_1$, $^7F_0 \rightarrow {}^5D_0$, $^7F_1 \rightarrow {}^5D_0$ transitions, respectively.

To determine the ligand triplet state, the Gd^{3+} analogous complex (Figure S1 in Supplementary material) luminescence spectra were performed at liquid nitrogen temperature (~77 K). The phosphorescence in this complex is assign to the ligand because the Gd^{3+} does not have transitions in this region. The emission spectrum of Gd^{3+} (Figure S2 in Supplementary material), when excited at the wide and intense absorption band presented at DR spectrum assigned to the IL and/or LMCT transitions.

The triplet state wavenumber (wavelength) value determined, $239.10^4\ cm^{-1}$ (419 nm) is consistent with a ligand to metal energy transfer mechanism since this ligand state is located at higher energy than the Eu^{3+} emission level [7,8].

The Eu^{3+} complex excitation spectrum, Fig. 6, present in the UV region, 270–300 nm, the wide band assigned to IL and/or LMCT and from 310 to 480 nm the narrow bands assigned in accord to [31] to f–f transitions, independently of the fixed emission wavelength, 615.5 nm or 618.5 nm.

In the Fig. 7 it is the Eu^{3+} complex emission spectrum where the $^5D_0 \rightarrow {}^7F_{0-4}$ at 580; 591, 594; 615.5, 618.5; 652; 688.5, 693, 698 nm are attributed. The low symmetry is responsible for the Stark splitting of the spin orbit levels. The uncommon observed $^5D_1 \rightarrow {}^7F_{0-2}$ transitions at 525 to 570 nm region, showed in the Fig. 7 expanded inset are assigned in accord to [31]. The same emission spectrum profile is observed in all spectra using 464, 361, 316.5, 300 e 275 nm excitations indicating that the same emission mechanism takes place. Remarkable is the europium emission intensity for the IL and/or LMCT excitations (275 and 300 nm) indicating a ligand sensitization mechanism, an antenna effect [30].

The $^5D_0 \rightarrow {}^7F_2$ transition is the most intense due to the low symmetry, without inversion center, of complex coordination metallic centers environment which is confirmed by the $^5D_0 \rightarrow {}^7F_2/{}^5D_0 \rightarrow {}^7F_1$ ratio intensity of about 2.8 [13]. The $^5D_0 \rightarrow {}^7F_1$ transition allowed by magnetic dipole mechanism, therefore less sensitive to the chemical environment was used to make intensity relationships. The presence of intense $^5D_0 \rightarrow {}^7F_4$ transition may be caused by the system rigidity provided by the binuclear complex.

The presence of $^5D_0 \rightarrow {}^7F_0$ transition in the room temperature emission spectra reveals that at least one europium symmetry site do not have an inversion center, since this transition is prohibited in microsymmetries with an inversion center [32]. An emission spectrum at 77 K temperature at the $^5D_0 \rightarrow {}^7F_0$ transition region was obtained (Fig. 8) to verify possible splittings. A band with a full width at half maximum (FWHM) ~32 cm^{-1} shows a shoulder at higher energy than the maximum energy position indicating that the europium ions have at least two symmetry sites but not so different to improve two $^5D_0 \rightarrow {}^7F_0$ independent transitions. Crystal-

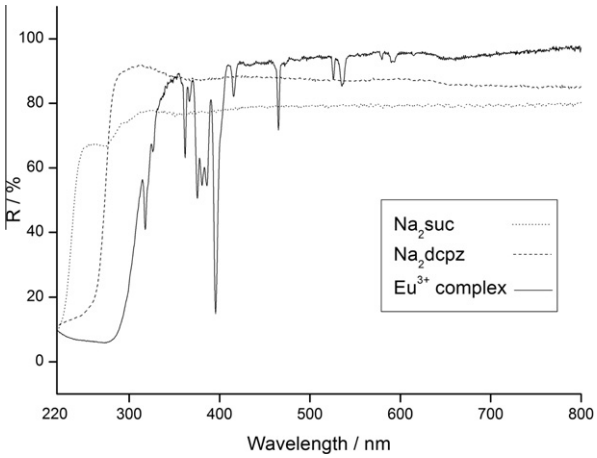

Fig. 5. Diffuse reflectance (DR) spectra of sodium succinate, sodium 3,5-dicarboxypyrazolate and Eu^{3+} complex.

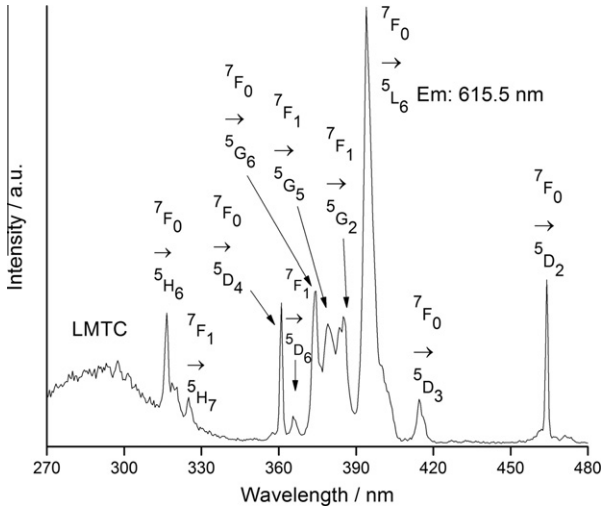

Fig. 6. Excitation spectrum of the Eu^{3+} complex (λ_{em} = 615.5 nm).

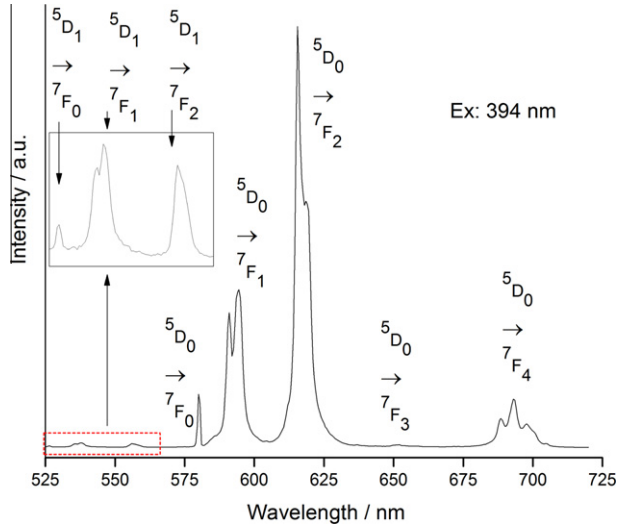

Fig. 7. Emission spectrum of the Eu^{3+} complex at room temperature (λ_{exc} = 394 nm).

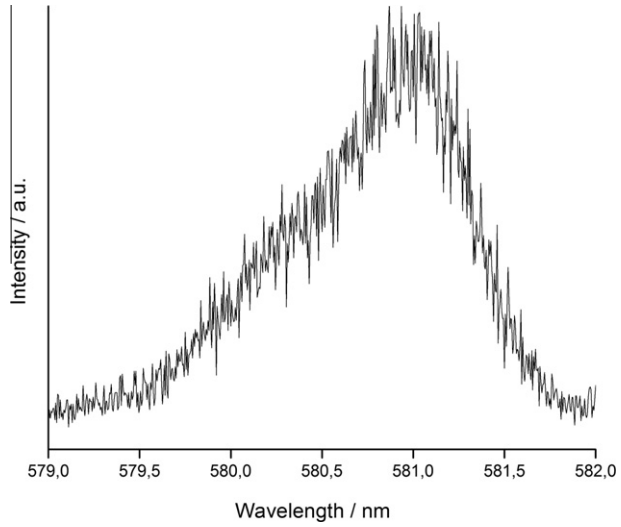

Fig. 8. Emission spectrum at 77 K (λ_{exc} = 394 nm) observing $^5D_0 \rightarrow {}^7F_0$ transition.

lographic results for the two europium centers of binuclear complex show small differences among the Eu-ligand bond distances, c.a. 0.01 a 0.04 Å (Table 2). An asymmetric shape with a shoulder of the $^5D_0 \rightarrow {}^7F_0$ is an example of the powerful probe properties of the Eu^{3+} ion.

The *x*, *y* CIE coordinates (from Comission Internationale L'Eclairage) from Eu^{3+} complex photoluminescence spectrum calculated [33] are *x* = 0.653 and *y* = 0.343 which is located in red region.

The excited state lifetime of the europium complex determined at room temperature with excitation at 394 nm and the emission monitored at 615.5 nm, is of 0.26 ms, whereas the compound $Eu(dcpz)(ox)_{0.5}(H_2O)_2]H_2O$ [12] present a lifetime of 0.44 ms.

This difference is largely determined by the greater number of the Eu^{3+} coordinated water in the $[Eu_2(dcpz)_2(suc)(H_2O)_8]\cdot(H_2O)_{1.5}$ complex, since water molecules vibrations are responsible for non-radiative deactivation process .

3.5. Thermogravimetric analysis

The complex stability was investigated using thermal analysis under air atmosphere from room temperature to 800 °C. Fig. 9

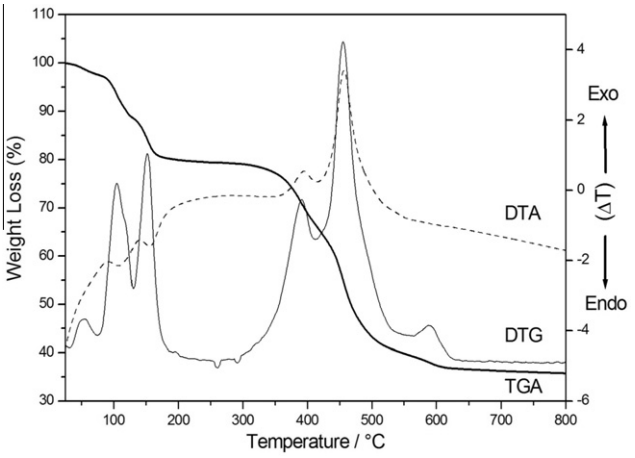

Fig. 9. TG, DTG and DTA curves for Eu^{3+} complex.

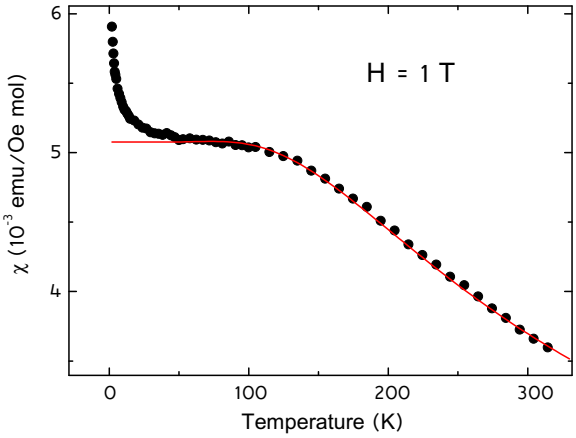

Fig. 10. Temperature dependence of the magnetic susceptibility measured with 1 T. The solid circles are the experimental data and the line is the calculated Van Vleck susceptibility from Ref. [35] with an energy splitting Δ/K_B = 475 K.

illustrate the TG, DTA and DTG curves obtained for the studied binuclear compound. The first mass loss of 3.01% corresponds to release of 1.5 uncoordinated water molecules in the temperature range 26–85 °C as it is evident from DTG curve peak with temperature maxima at 55 °C (Obsd: 3.01%, Calcd: 3.00%). In this case, the weight loss is slow and cannot be detected in the DTA curve. Both second and third endothermic steps (centered at 106 and 152 °C, respectively) correspond to the release of eight coordinated water molecules (Obsd: 16.05%, Calcd: 16.02%). The fourth exothermic step centered at 392 °C accounts for the release of one suc^- ligand (Obsd: 12.94%, Calcd: 12.89%). Decomposition of other organic moiety takes place in the fifth and sixth exothermic steps (centered at 456 and 592 °C, respectively) and it is attributed to the release of two $dcpz^{2-}$ ligands (Obsd: 32.1%, Calcd: 34.2%). In addition the residual percentage weight at 800 °C is consistent with the formation of one mol of Eu_2O_3 (Obsd: 35.89%, Calcd: 39.1%).

3.6. Magnetic behavior

Fig. 10 shows the temperature dependence of the dc magnetic susceptibility of the europium complex. The most prominent feature is the approximately temperature independent behavior of the susceptibility below 100 K. The ground state of Eu^{3+} has zero total angular momentum (*J* = 0) and the contribution to the suscep-

tibility comes from the higher multiplets since the separation between the ground state and the first excited state is comparable to the thermal energy. The mixing of excited states is responsible for the observed weak temperature dependence of the susceptibility known as Van Vleck paramagnetism [34]. In order to fit the data we use the calculation in Ref. [35]:

$$\chi = \frac{N\mu_B^2}{z}\left(\frac{A}{3\Delta}\right)$$

$$Z = 1 + 3e^{-\Delta/k_BT} + 5e^{-2\Delta/k_BT}7e^{-6\Delta/k_BT} + 9e^{-10\Delta/k_BT} + 11e^{-15\Delta/k_BT} + 13^{-21\Delta/k_BT}$$

$$A = 24 + \left(13.5\frac{\Delta}{K_BT} - 1.5\right)e^{-\Delta/K_BT} + \left(67.5\frac{\Delta}{K_BT} - 2.5\right)e^{-3\Delta/K_BT} + \left(189\frac{\Delta}{K_BT} - 3.5\right)e^{-6\Delta/K_BT} + \left(405\frac{\Delta}{K_BT} - 4.5\right)e^{-10\Delta/K_BT} + \left(742.5\frac{\Delta}{K_BT} - 5.5\right)e^{-15\Delta/K_BT} + \left(1228.5\frac{\Delta}{K_BT} - 6.5\right)e^{-21\Delta/K_BT}$$

Here N is the number of Eu^{3+} ions and μ_B is the Bohr magneton. This expression for the paramagnetic susceptibility has only one unknown parameter, the energy splitting Δ/K_B between $J = 0$ and $J = 1$ states for Eu^{3+}. As can be seen in the Fig. 10 the theoretical prediction using $\Delta/K_B = 475$ K is in very good agreement with the experimental data for a broad temperature range from 314 K to about 70 K. We note that a very similar energy splitting $\Delta/K_B = 471$ K was found in Ref. [35] for the compound $EuBO_3$. The actual value of Δ/K_B depends on the environment of the Eu ion due to crystalline field effects. Finally, we discuss the fast increase in X below ~30 K. Several inorganic europium compounds present similar low temperature increase in the susceptibility that is usually associated to a small amount of Eu^{2+} impurity [35,36]. The synthesis conditions of our coordination compound on the other hand exclude this possibility since it is extremely difficult to stabilize Eu^{2+} starting from the aqueous solution at room temperature. A better explanation would be the presence of a small amount of other rare earths ions, most probably Gd^{3+} ($4f^7$), in the europium precursor used in the synthesis.

4. Conclusions

The new binuclear complex $[Eu_2(dcpz)_2(suc)(H_2O)_8]\cdot(H_2O)_{1.5}$ has been prepared by green synthetic strategy using succinate anion and 3,5-dicarboxypyrazolate as multifunctional bridging ligands. Intramolecular $\pi\cdots\pi$ and $NH\cdots O$ interactions are observed. Two adjacent species are connected via hydrogen bonds generating a 3D supramolecular framework. The compound exhibits the characteristic emission of europium ions, showing that the ligands are luminescence sensitizers. The Eu^{3+} emission shows characteristic lines of two sites with very similar symmetries in accordance with with crystallographic data. The magnetic susceptibility is analyzed on the basis of the Van Vleck paramagnetic theory and an energy splitting of $\Delta/K_B = 475$ K was obtained.

Acknowledgments

The authors thank the Brazilian agencies CNPq, CAPES and FAPESP for financial support.

Appendix A. Supplementary material

CCDC 903053 contains the supplementary crystallographic data for $[Eu_2(dcpz)_2(suc)(H_2O)_8]\cdot(H_2O)_{1.5}$. These data can be obtained free of charge via http://www.ccdc.cam.ac.uk/conts/retrieving.html, or from the Cambridge Crystallographic Data Centre, 12 Union Road, Cambridge CB2 1EZ, UK; fax: +44 1223 336 033; or e-mail: deposit@ccdc.cam.ac.uk. Supplementary data associated with this article can be found, in the online version, at http://dx.doi.org/10.1016/j.poly.2013.01.031.

References

[1] A.R. Ramya, M.L.P. Reddy, A.H. Cowley, K.V. Vasudevan, Inorg. Chem. 49 (2010) 2407.
[2] J.D. Rocca, W. Lin, Eur. J. Inorg. Chem. (2010) 3725.
[3] A. Kitai (Ed.), Luminescent Materials and Applications, Wiley, Chichester, 2008.
[4] J. Rocha, L.D. Carlos, F.A.A. Paz, D. Ananias, Chem. Soc. Rev. 40 (2011) 926.
[5] T. Jüstel, H. Nikol, C. Ronda, Angew. Chem., Int. Ed. 37 (1998) 3084.
[6] G. Zucchi, O. Maury, P. Thuéry, M. Ephritikhine, Inorg. Chem. 47 (2008) 10398.
[7] L. Armelao, S. Quici, F. Barigelletti, G. Accorsi, G. Bottaro, M. Cavazzini, E. Tondello, Coord. Chem. Rev. 254 (2010) 487.
[8] G.F. de Sa, O.L. Malta, C. de Mello Donega, A.M. Simas, R.L. Longo, P.A. Santa-Cruz, E.F. da Silva Jr., Coord. Chem. Rev. 196 (2000) 165.
[9] L. Dong, Y. Tian, X. Li, Y. Jiang, J. Coord. Chem. 63 (2010) 2088.
[10] C.B. Aakeröy, A.M. Beatty, Aust. J. Chem. 54 (2001) 409; S. Kitagawa, K. Uemura, Chem. Soc. Rev. 34 (2005) 109.
[11] D. Min, S.W. Lee, Inorg. Chem. Commun. 5 (2002) 978.
[12] H. Wu, S. Yue, N. Wang, Y. Liu, J. Coord. Chem. 63 (2010) 785.
[13] G. Zhang, W. Zhang, Z. Han, Chem. Comm. 12 (2009) 982.
[14] J. Xia, B. Zhao, H.-S. Wang, W. Shi, Y. Ma, H.-B. Song, P. Cheng, D.-Z. Liao, S.-P. Yan, Inorg. Chem. 46 (2007) 3450.
[15] S.C. Manna, E. Zangrando, A. Bencini, C. Benelli, N.R. Chaudhuri, Inorg. Chem. 45 (2006) 9114.
[16] B. Yu, C. Xie, X. Wang, R. Wang, G. Shen, D. Shen, J. Coord. Chem. 60 (2007) 1817.
[17] Enraf-Nonius, COLLECT, Nonius BV, Delft, The Netherlands, 1997–2000.
[18] Z. Otwinowski, W. Minor, H.K.L. Denzo, in: C.W. Carter Jr., R.M. Sweet (Eds.), Methods in Enzymology, vol. 276, Academic Press, New York, 1997.
[19] P. Coppens, L. Leiserowitz, D. Rabinovich, Acta Crystallogr. 18 (1965) 1035.
[20] G.M. Sheldrick, Acta Crystallogr. A64 (2008) 112.
[21] L.J. Farrugia, J. Appl. Crystallogr. 30 (1997) 565.
[22] K. Momma, F. Izumi, J. Appl. Crystallogr. 44 (2011) 1272.
[23] A.L. Spek, J. Appl. Crystallogr. 36 (2003) 7.
[24] J. Klingele, S. Dechert, F. Meyer, Coord. Chem. Rev. 253 (2009) 2698.
[25] L. Pan, X. Huang, J. Li, Y. Wu, N. Zheng, Angew. Chem., Int. Ed. 39 (2000) 527.
[26] C. Janiak, J. Chem. Soc., Dalton Trans. 21 (2000) 3885.
[27] G.R. Desiraju, Angew. Chem., Int. Ed. 46 (2007) 8342.
[28] G.B. Deacon, R.J. Phillips, Coord. Chem. Rev. 33 (1980) 227.
[29] L.S. Lima, F.J. Caires, C.T. Carvalho, A.B. Siqueira, M. Ionashiro, Termochim. Acta. 501 (2010) 50.
[30] N. Sabbatini, M. Guardigl, Coord. Chem. Rev. 123 (1993) 201.
[31] W.T. Carnall, P.R. Fields, K. Rajnak, J. Chem. Phys. 49 (1968) 4412.
[32] J.-C.G. Bünzli, G.R. Choppin, Lanthanide Probes in Life, Chemical a Earth Sciences: Theory and Practice, Elsevier, Amsterdam, 1989. 234p.
[33] P.A. Santa-Cruz, F.S. Teles, Spectra Lux Software v. 1.0, Ponto Quântico Nanodispositivos/RENAMI, 2003.
[34] J.H. Van Vleck, The Theory of Electric and Magnetic Susceptibilities, Oxford University Press, Oxford, 1932.
[35] Y. Takikawa, S. Ebisu, S. Nagata, J. Phys. Chem. Solids 71 (2010) 1592.
[36] B.J. Ruck, H.J. Trodahl, J.H. Richter, J.C. Cezar, F. Wilhelm, A. Rogalev, V.N. Antonov, Binh Do Le, C. Meyer, Phys. Rev. B 83 (2011) 174404-1.